Biosensors and Bioelectronics 173 (2021) 112785

Contents lists available at ScienceDirect

Biosensors and Bioelectronics

journal homepage: http://www.elsevier.com/locate/bios

A novel dual signal and label-free electrochemical aptasensor for mucin 1 based on hemin/graphene@PdPtNPs

Guojuan Zhang, Zhiguang Liu, Lifang Fan, Yujie Han, Yujing Guo *

Institute of Environmental Science, Shanxi University, Taiyuan, 030006, China

ARTICLE INFO

Keywords:
Graphene
Hemin
PdPtNPs
Dual signal electrochemical aptasensor
Mucin 1

ABSTRACT

A dual signal and label-free electrochemical aptasensor for mucin 1 was constructed based on hemin/graphene@PdPtNPs nanocomposite (H-Gr@PdPtNPs). Hemin attached on the graphene surface not only improves the solubility of graphene and acts as an in-situ electrochemical probe but also exhibits excellent peroxidase-like properties to electrocatalyze the reduction of H_2O_2. PdPtNPs also show outstanding catalytic capacity to the reduction of H_2O_2 and provide numerous binding sites for loading dDNA (mucin 1 aptamer and cDNA) to form the sensing interface. In the presence of mucin 1, due to the specific affinity between aptamer and mucin 1, double helix would be induced dissociation and the aptamer would be pulled off from the electrode. As a result, the electrochemical signals of hemin and H_2O_2 were recovered. Based on these properties, the label-free and sensitive dual signal electrochemical biosensor for mucin 1 detection has been developed. The one is differential pulse voltammetry (DPV) signal of hemin and the other is chronoamperometry signal arisen from the catalytic reduction of H_2O_2. The linear ranges for mucin 1 were 8.0 pg mL^{-1} to 80 ng mL^{-1} and 0.8 pg mL^{-1} to 80 ng mL^{-1} with the limit of detection 2.5 pg mL^{-1} and 0.25 pg mL^{-1} by DPV and chronoamperometry, respectively. The recovery of mucin 1 in human blood serum samples was from 95.0% to 104.2%. The detection platform does not need signal labeling which greatly reduced the sophisticated and expensive procedures. The aptasensor provide a promising strategy for the determination of mucin 1 in clinical diagnostics.

1. Introduction

Mucin 1 is a membrane-associated glycoprotein abnormally over-expressed in the majority of human malignancies and considered as a predominant protein biomarker in adenocarcinomas (breast, ovarian, prostate, and pancreatic cancers) (Kufe 2009). Clinical cut off level for mucin 1 in healthy human serum was deemed to be 30 U·mL^{-1} (5.0 μmol L^{-1}) and under 30 U·mL^{-1} was generally reported as the normal level (Cheng et al., 2009). A higher mucin 1 level may usually indicate the possibility of malignancies and 100 fold amount increase of mucin 1 is indicative greater presence of cancer (Gheybi et al., 2014). Particularly, it has been a reliable biomarker for the diagnosis of human cancers in the early stages (Apostolopoulos et al., 2006). Therefore, detection and quantification of mucin 1 is quite essential in clinical diagnostics. To date, various techniques have been used to enhance the detection performance, such as electrochemical aptasensor (Hatami et al., 2019; Wang et al., 2017), fluorescence (Cao et al., 2019), enzyme linked immunosorbent assay (ELISA) (Falahat et al., 2015), colorimetry (Liu et al., 2018a) etc. Among these techniques, electrochemical aptasensor has drawn considerable attentions because it combines the distinct properties of low cost and simple device portability of electrochemical methods with the high affinity and specificity of aptamers. For instance, a cDNA-Fc/Ti_3C_2 probe was executed to develop a competitive electrochemical aptasensor by Wang's group and achieved sensitive detection of mucin 1 (Wang et al., 2020). An Exo III-assisted triple-amplified electrochemical aptasensor was constructed by Zheng's group with highly sensitivity for mucin 1 detection (Zheng et al., 2019). Target recycling amplification strategy and effective MoS_2 nanoflower-based signal probe were employed to manufacture an electrochemiluminescent assay for mucin 1 (Li et al., 2018). Hence, electrochemical aptasensor is considered as a reliable, cost saving and efficient method for target analysis.

The important factor to improve sensitivity of electrochemical sensors relies on the electrode materials. Graphene, with its large theoretical surface area, remarkable electrical conductivity and high mechanical properties make it an excellent candidate for fabricating electrochemical sensing platform (Kimmel et al., 2012). It is also considered as a fixed matrix which can interact with a broad range of

* Corresponding author.
E-mail address: guoyj@sxu.edu.cn (Y. Guo).

https://doi.org/10.1016/j.bios.2020.112785
Received 28 August 2020; Received in revised form 13 October 2020; Accepted 30 October 2020
Available online 4 November 2020

functional molecules through Van Der Waals force, π-π stacking, electrostatic interaction or covalent bonding (Nie et al., 2019). Hemin, a well-known iron porphyrin can be adsorbed on the surface of graphene via π-π interactions to form hemin functionalized graphene nanosheets (H-Gr). In the nanocomposite, hemin can be used as electron media ascribing to the reversible redox of Fe(III)/Fe(II) (Guo et al., 2011b). It also has the peroxidase-like capacity which can catalyze H_2O_2 decomposition (Liu et al., 2016). Here, electrochemical signal of H_2O_2 can also be considered as a mediator to monitor the target indirectly (Wang et al., 2019). Based on the above properties, the in-situ probe of reversible $hemin_{ox}/hemin_{red}$ pair and the catalytic signal of H_2O_2 can be served as the dual signal to realize the electrochemical detection. Dual signal strategy could be mutual corroboration, which effectively avoid producing false positive or false negative results to great extent. Until now, lots of dual signal sensors were ingeniously designed and used for sensitive detection. A delicate immunosensor with brilliant photoelectrochemical and photothermal dual signal was successfully constructed by Wang's group (Wang et al., 2019), and dual-electrochemical signal aptasensor fabricated by Xu's group achieved the ultrasensitive detection of malathion (Xu et al., 2019). The proposed dual signal sensors featuring with good accuracy and high reliability not only can make the analytical results more convinced than traditional single-readout mode but also greatly improve the sensitivity, robustness and repeatability of the sensor.

Gr-based nanomaterials demonstrated higher electrocatalytic activity, more favorable electron transfer kinetics and enhanced electrochemical reactivity than graphene itself. They provided more robust and advanced electrode material for sensing platform. The electrochemical aptasensor can be further improved through combining graphene with other nanomaterials, including noble metal nanoparticles (NPs), metal oxide, conducting polymers (Song et al., 2019). Among them, bimetallic NPs exhibits the superiority of outstanding intrinsic electrocatalytic capacity, inherent biocompatibility and larger specific surface area over the corresponding monometallic NPs in virtue of the synergetic effect, which are in extensive demand in the field of sensing in particular (Chen et al. 2019, 2020). More recently, Pt–Pd alloy nanostructures were introduced to test electrocatalytic activities toward formic acid oxidation (Zhang et al., 2012). ZIF-8-rGO supported bimetallic AuPtNPs acted as a synergistic catalyst for H_2O_2 detection (Zhang et al., 2019). AuPdNPs served as a platform for aptamers conjugating via Au-thiol bond to capture cancer cells and as a catalyst for the ECL reaction of H_2O_2 to detect cancer cells based a disposable paper analytical device (Ge et al., 2018). The non-enzyme direct electrochemical sensing of H_2O_2 by nanostructure containing bimetallic PtAuNPs supported on silica nanorods and the non-supported PtAuNPs is reported by Liu's group (Liu et al., 2018b). Thus, introduction of bimetal nanostructures can not only enhance synergistic catalysis to improve the sensitivity effectively, but also anchor aptamers to perfect the selectivity of the electrochemical sensors.

In this work, a dual signal enhanced mucin 1 aptasensor was constructed based on the synthesized H-Gr@PdPtNPs. The nanocomposite combining the unique properties of H-Gr and PdPtNPs exhibits excellent peroxidase-like capacity, good electrical conductivity, and large specific surface area. It also can provide binding sites for dDNA (designed by the mucin 1 aptamer and its complementary strand) firmly assembling on the modified electrode and possess good catalytic ability to promote the decomposition of H_2O_2. The signals of hemin and the catalytic capacity for H_2O_2 sharply reduced due to the dDNA attaching. In the presence of mucin 1, dDNA structural switching induced by mucin 1 binding to aptamer specifically and most aptamers were pulled off from electrode surface. Thus, the electrochemical signals of hemin and the catalytic activity to H_2O_2 were partially recovered. The signals enhancement for the peak currents of hemin and H_2O_2 can be as indicators for mucin 1 determination. The results demonstrated that sensing platform had wide linear range, low detection limit, high selectivity, and reproducibility. The aptasensor was also employed to detect mucin 1 in human serum samples and shown satisfied recoveries. These results indicate the sensing platform can be a candidate in the field of clinical diagnosis.

2. Materials and methods

2.1. Materials and instruments

Graphite powder was obtained from Alfa Aesar. PDDA (Poly dimethyl diallyl ammonium chloride, Mw = 400,000–500,000, 10 wt% in water), prostate specific antigen (PSA), bovine serum albumin (BSA), human serum albumin (HSA), lysozyme (Lys), hemin, hemoglobin (Hb), intravenous gamma globulin (IgG), carcinoembryonic antigen (CEA), uric acid (UA), ascorbic acid (AA) and L-tyrosine (L-Tyr) were supplied from Sigma-aldrich Co. (Louis, USA). $CaCl_2$, $FeCl_3$, Tri-HCl, NaCl, KCl, $MgCl_2$, K_2PdCl_4, $H_2PtCl_6{\cdot}6H_2O$ and $HAuCl_4{\cdot}4H_2O$ were obtained from Aladdin-reagent Co. (Shanghai, China). The human serum samples were provided by the local hospital. Mucin 1 peptide: APDTRPAPG (Chen et al., 2015; Yang et al., 2018), its corresponding aptamer (MUC 1a): 5′-GCA GTT GAT CCT TTG GAT ACC CTG G-3′ (Jiang et al., 2017; Ma et al., 2018), complementary strand of the aptamer (cDNA): 5′–NH_2–$(CH_2)_6$-CGT CAA CTA GGA AAC CTA TGG GAC C-3′, insulin peptide (SHLVEALYLVCGERG), mucin 4, mucin 16 and mucin 20 were purchased from Shanghai Sangon Biotech Co., Ltd. (Shanghai, China). All the biomolecules were dissolved in Tris-buffer (20 mmol L^{-1} Tri-HCl, 0.10 mol L^{-1} NaCl, 5.0 mmol L^{-1} $MgCl_2$, pH = 7.4). All reagents were analytical grade, and the distilled water used in the entire experiment was derived from the Millipore system supplied by Millipore water Ltd. (18.2 MΩ cm, USA).

The morphology of the nanocomposite was recorded on a JEOL-2100 TEM (Electron Ltd., Tokyo, Japan) with an accelerating voltage of 200 kV. X-ray photoelectron spectroscopy (XPS) measurement was performed on an ESCALAB-MKII 250 photoelectron spectrometer (VG Co., New York, USA) with Al Kα X-ray radiation as the X-ray source for excitation. Electrochemical measurements were conducted on a Princeton Applied Research (PAR 4000, PMl-500) Workstation (AMETEK princeton applied research.com, America) with a conventional three electrodes system composed of a glassy carbon electrode (GCE, Φ = 3.0 mm), a platinum column electrode (Φ 1.0 mm × 10 mm) and a saturated calomel electrode (SCE), as the working electrode, the counter electrode and the reference electrode respectively.

2.2. Preparation of H-Gr@PdPtNPs

The graphite oxide (GO) was prepared from graphite powder by the modified Hummers' method (Hummers and Offeman 1958). H-Gr was synthesized on the basis of the literature (Guo et al., 2011a). Typically, 2.5 mL GO dispersion (1.0 mg mL^{-1}) was mixed with the 2.5 mL equivalent concentration of hemin, then 100 μL of ammonia (25 wt%) and 10 μL of hydrazine solution (80 wt%) were added into the above miscible liquids. The mixture was heated at 60 °C for 4 h. Then, the suspension was centrifuged at 12,000 rpm for 20 min to obtain H-Gr.

H-Gr@PdPtNPs was synthesized by the reduction of K_2PdCl_4 and $H_2PtCl_6{\cdot}6H_2O$ with fresh $NaBH_4$ solution. Concretely, 50 μL PDDA was mixed with 2.0 mL H-Gr (0.25 mg mL^{-1}) aqueous dispersion in a 10 mL flask and stirred for a couple of minutes. Then, 65 μL 10 mg mL^{-1} K_2PdCl_4 and 97 μL 10 mg mL^{-1} $H_2PtCl_6{\cdot}6H_2O$ were added into the flask. After that, 2.0 mL $NaBH_4$ solution (20 mmol L^{-1}) was slowly dropped in the mixture. After rapidly stirred for half an hour, the product was centrifuged at 8000 rpm for 15 min and washed twice with Milli-Q water. Then, the H-Gr@PdPtNPs composite was obtained. In order to reveal the electrochemical catalytic performance of H-Gr@PdPtNPs, the related nanomaterials such as H-Gr@AuNPs, H-Gr@PdNPs, H-Gr@PtNPs, H-Gr@AuPdNPs, H-Gr@AuPtNPs have also been prepared. The details were descripted in the supporting materials.

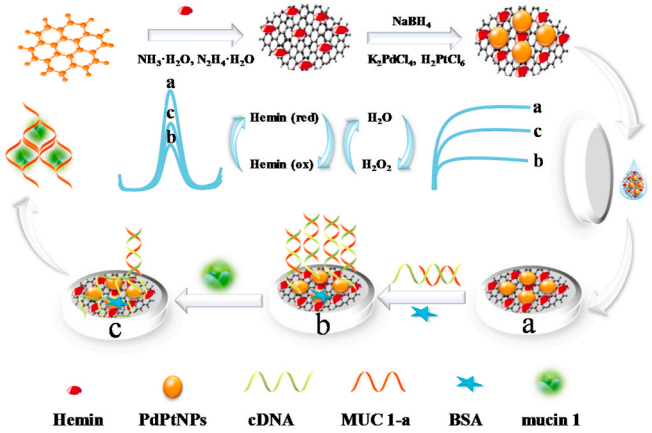

Scheme 1. The procedure for the synthesis of H-Gr@PdPtNPs and the dual signal electrochemical aptasensor for mucin 1 detection.

2.3. Fabrication of the aptasensor

The bare GCE was preconditioned carefully using 0.03 μm and 0.05 μm alumina powder to remove the surface dirt, and then, 9.0 μL of 0.25 mg mL^{-1} H-Gr@PdPtNPs dispersion was drop-casted onto the GCE to obtain H-Gr@PdPtNPs/GCE. Subsequently, 10 μL of 4.0 μmol L^{-1} hybridization dDNA (obtained by mixing 8 μmol L^{-1} MUC 1a with equal volume of 8 μmol L^{-1} cDNA and incubating at 37 °C water bath about 3 h) was placed on the H-Gr@PdPtNPs/GCE surface and preserved at 4 °C overnight. After that, the resulting electrode was submerged in 1.0% BSA for 30 min to block the possible remaining active sites and avoid nonspecific adsorption. Finally, the sensing interface of dDNA/H-Gr@PdPtNPs/GCE was fabricated successfully.

2.4. Mucin 1 detection

First, DPV and chronoamperometry responses of the dDNA/H-Gr@PdPtNPs/GCE were carried out in 0.10 mol L^{-1} PBS (pH = 7.4, 0.10 mol L^{-1} KCl) without or with 3.0 mmol L^{-1} H_2O_2 to obtain the initial peak current, respectively. Afterward, 5 μL mucin 1 standard solutions at different concentrations were successively injected into 5 mL 0.10 mol L^{-1} PBS supporting electrolyte and incubated with dDNA/H-Gr@PdPtNPs/GCE for 40 min at room temperature. The dual electrochemical techniques were employed to monitor the recognition of mucin 1 by measuring the peak currents of hemin and H_2O_2, respectively. The experiments were performed in the potential range from −0.8 V to 0 V with the amplitude of 50 mV, pulse width of 0.050 s and step potential 5.0 mV.

3. Results and discussion

3.1. Detection strategy

Scheme 1 depicts the dDNA/H-Gr@PdPtNPs/GCE fabrication and sensing procedure for the dual signal detection. Firstly, hydrothermal method was applied for H-Gr preparation under alkaline atmosphere (Guo et al., 2011a). The introduction of hemin not only can keep graphene away from coagulation and act as in-situ probe owing to the reversible $hemin_{ox}$/$hemin_{red}$ pair, but also endow graphene with peroxidase activity which showed excellent electrocatalysis for the reduction of H_2O_2. Then, PdPtNPs was loaded onto the H-Gr by reduction of K_2PdCl_4 and $H_2PtCl_6{\cdot}6H_2O$ with fresh $NaBH_4$ to obtain H-Gr@PdPtNPs. The existence of PdPtNPs not only can provide more binding sites for dDNA self-assembly but also accelerate the reduction of H_2O_2 owing to the peroxidase activity (Fan et al., 2019). After that, H-Gr@PdPtNPs were dropped on the surface of GCE to obtain H-Gr@PdPtNPs modified GCE (H-Gr@PdPtNPs/GCE). Subsequently, dDNA was assembled on the H-Gr@PdPtNPs/GCE to obtain the sensing interface dDNA/H-Gr@PdPtNPs/GCE. The immobilization of dDNA on the H-Gr@PdPtNPs surface would be an obstacle which hinder the electron transfer of hemin and reduce the nanoenzyme's peroxidase activity. In the presence of mucin 1, the MUC 1a would recognize mucin 1 to form mucin 1-MUC 1a complex (Xiang et al., 2017) and then the complex separated from the electrode. As a result, there was less biomolecule on the sensor surface, the signals of hemin and electrocatalytic property to H_2O_2 recovered partially. The DPV and chronoamperometry signals increased linearly with the increase of mucin 1 concentration. Thus, a dual signal and label-free electrochemical aptasensor has been constructed for the detection of mucin 1.

3.2. Characterization of H-Gr@PdPtNPs

H-Gr has been characterized by UV–vis and FT-IR spectra in our preliminary work (Zhang et al., 2018). The Morphology of the prepared H-Gr@PdPtNPs was studied by TEM. As shown in Fig. 1A, the flake-like morphology with wrinkled topology is the typical images of H-Gr. PdPtNPs with a mean size of 10 nm are evenly loaded on the H-Gr surface. HRTEM image in Fig. 1B shows two types of lattice fringes 0.229 nm and 0.201 nm, which can be indexed to the {111} and {200} lattice spacing of Pd–Pt alloy respectively. Moreover, the result of EDS also shows that the nanoparticles consist of Pd and Pt and the atomic ratio of Pd/Pt are 51% to 49% (Fig. S2).

Besides, XPS were performed to analysis the element composition along with the oxidation states of H-Gr@PdPtNPs. The survey of H-Gr@PdPtNPs (Fig. 1C) shows the presence of C1s and O1s arise from Gr, Fe2p at 712 eV and N1s at 400 eV originate from hemin, the presence of Pt4f and Pd3d belongs to PdPtNPs. As can be seen in Fig. 1D, C–C (284.5 eV), C–N (285.4 eV), C–O (286.3 eV), C═O (287.3 eV) and O–C═O (288.6 eV) stand for five kinds of carbon bonds in the C1s spectrum (Wang et al., 2015). The peak of Pd3d appears at 335 eV (Fig. 1E). $Pt4f_{5/2}$ and $Pt4f_{7/2}$ appear at 75 eV and 72 eV, respectively in Fig. 1F (Mourya et al., 2019). All of the results demonstrated that H-Gr@PdPtNPs has been synthesized perfectly.

3.3. Electrochemical characterization of the aptasensor

DPV and chronoamperometry were investigated to illustrate the fabrication process of the dDNA/H-Gr@PdPtNPs/GCE. As shown in Fig. 2A, the DPV of H-Gr/GCE displays obvious oxidation peak at −0.362 V (Fig. 2A curve a) which attributed to the oxidation of hemin. Meanwhile, H-Gr/GCE exhibits strong electrocatalytic property to H_2O_2 owing to peroxidase-like capacity of hemin (Fig. 2B, curve a). Compared with H-Gr/GCE, H-Gr@PdPtNPs/GCE exhibits a very fast charge transfer process and dramatic electrocatalytic property (curve b) which is due to the peroxidase-like capacity of PdPtNPs and the synergistic catalytic effect between H-Gr and PdPtNPs. After assembling of dDNA and BSA on the H-Gr@PdPtNPs/GCE surface, the currents declined continuously (curve c, d) which may attribute to the insulated biomolecules hindering the electron transfer of hemin and reducing the electrocatalytic activity. Afterward, the addition of 3.0 ng mL^{-1} mucin 1 resulted in an increase in current peak (curve e) confirming the successful specific recognition between mucin 1 and MUC1a, and the formed mucin 1-MUC1a complex was away from the electrode. As a result, the electron transfer rate was recovered, leading to an enhancement of hemin signal and electrocatalytic property to H_2O_2. These stepwise characteristics demonstrate that the sensing surface of the dual signal on detection for mucin 1 is successfully fabricated.

3.4. Optimization of the experimental condition

Some experimental parameters affecting the sensitivity of the electrochemical sensor have been optimized, such as the precursor ratio of

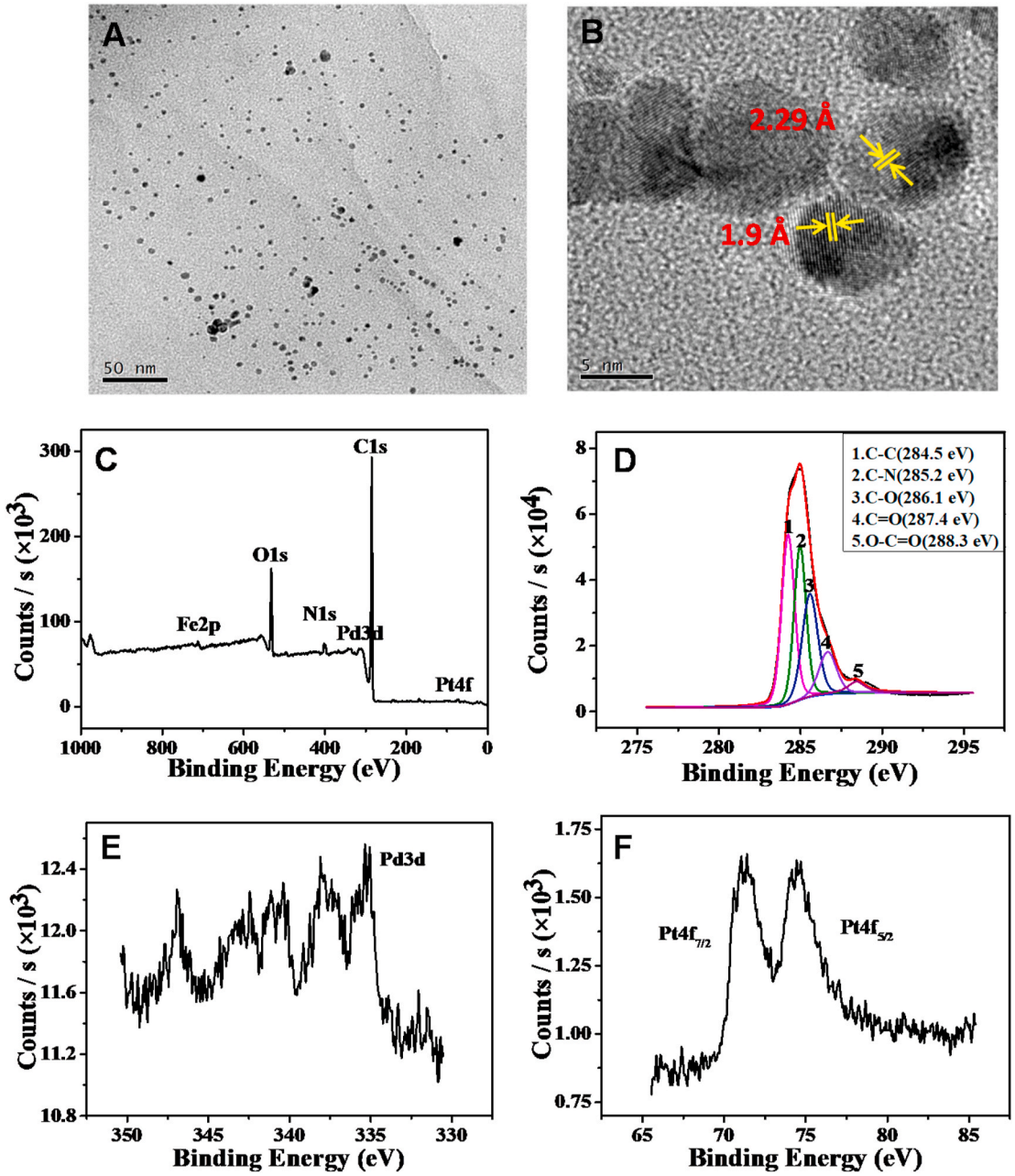

Fig. 1. (A) The TEM images of H-Gr@PdPtNPs; (B) HRTEM of H-Gr@PdPtNPs; (C)The XPS spectra of H-Gr@PdPtNPs, (D) C1s, (E) Pd3d and (F) Pt4f.

Pd/Pt, the modified amount of H-Gr@PdPtNPs, the concentration of dDNA, and the incubation time. The details are as follows.

In order to display the best catalytic performance, H-Gr@PdPtNPs with different precursor ratio of Pd/Pt (2:1, 1:1, 1:2) were investigated by DPV. As shown in Fig. S3, H-Gr@PdPtNPs presented a higher peak current at the ratio of 1:1 which probably due to the same ratio of Pd/Pt exhibited greater current densities and electrochemical active surface areas (Themsirimongkon et al., 2018). Therefore, a Pd/Pt precursor ratio of 1:1 was selected as the optimum ratio for H-Gr@PdPtNPs preparation.

Another parameter which affects the sensitivity of the sensor is the modification volume of H-Gr@PdPtNPs. As shown in Fig. S4 (A), the peak current increased with the increase of H-Gr@PdPtNPs (0.25 mg mL^{-1}) from 4.0 μL to 9.0 μL and then reduced obviously when it is exceeded 9.0 μL. The finding could ascribe to thick coating blocking the electrons transfer. Thus, the optimized modification volume of H-Gr@PdPtNPs was determined as 9.0 μL.

In addition, the effect of the concentration of dDNA was studied. As shown in Fig. S4 (B), the peak current of hemin reduced evidently when the concentration of dDNA increased from 0.5 μmol L^{-1} to 4.0 μmol L^{-1}. Then the signal began to leave off indicating that saturated dDNA were captured on the electrode surface. Thus, 4.0 μmol L^{-1} dDNA was selected for sensor fabrication.

At last, incubation time between dDNA and mucin 1 was investigated. When dDNA/H-Gr@PdPtNPs/GCE was immerging into 80 ng mL^{-1} mucin 1 solution, MUC1a was captured by mucin 1 via specific binding and mucin 1-MUC 1a separated from the cDNA. As illustrated in Fig. S4 (C), the signal increased gradually with the incubation time and reached a plateau at 40 min. As a result, 40 min was used as the optimal incubation time for the assay.

3.5. The electrochemical dual signal performance

Under the optimized conditions, the responses of dDNA/H-

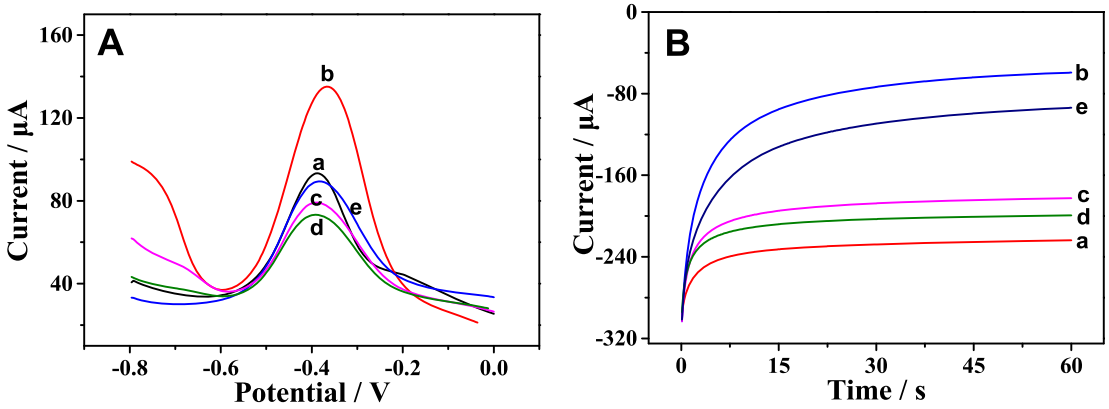

Fig. 2. (A) DPV of H-Gr/GCE (a), H-Gr@PdPtNPs/GCE (b), dDNA/H-Gr@PdPtNPs/GCE (c), BSA/dDNA/H-Gr@PdPtNPs/GCE (d), BSA/dDNA/H-Gr@PdPtNPs/GCE in PBS containing 3.0 ng mL^{-1} mucin 1(e); (B) Chronoamperometry of H-Gr/GCE (a), H-Gr@PdPtNPs/GCE (b), dDNA/H-Gr@PdPtNPs/GCE (c), BSA/dDNA/H-Gr@PdPtNPs/GCE (d), BSA/dDNA/H-Gr@PdPtNPs/GCE in PBS containing 3.0 ng mL^{-1} mucin 1 and 3.0 mmol L^{-1} H_2O_2 (e).

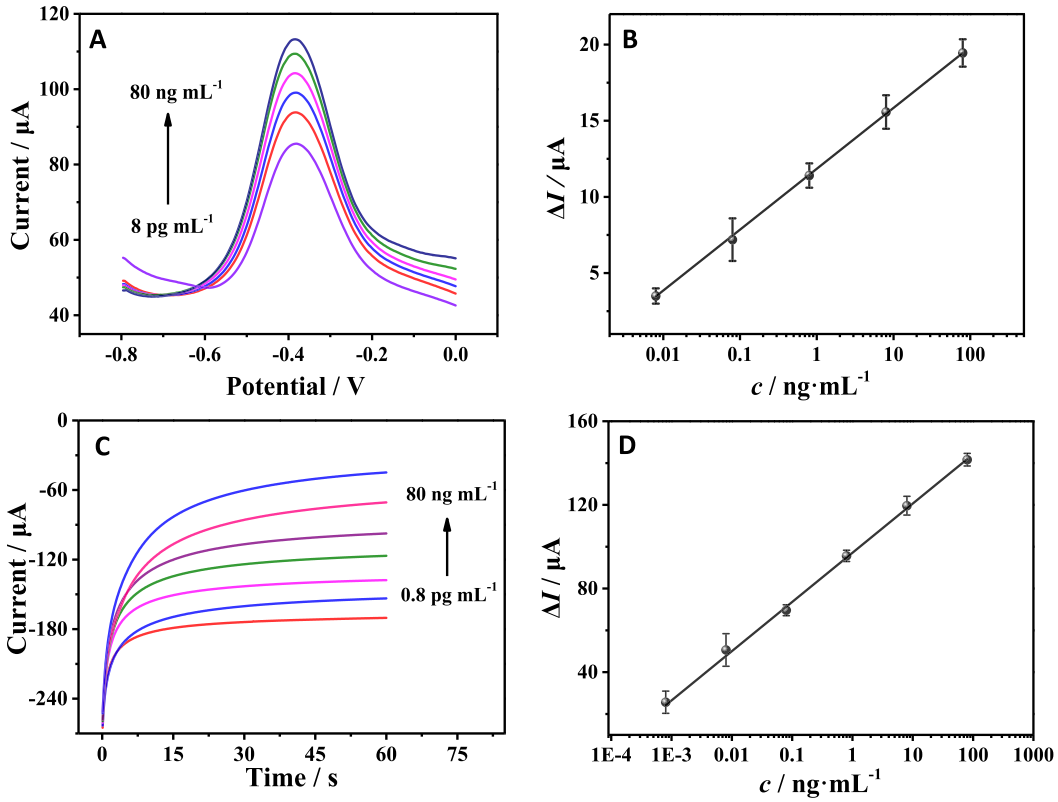

Fig. 3. (A) DPV of the aptasensor for different concentrations of mucin 1 in PBS (0, 0.008, 0.08, 0.8, 8, 80 ng mL^{-1}); (C) Chronoamperometry of the aptasensor for different concentrations of mucin 1 (0, 0.0008, 0.008, 0.08, 0.8, 8, 80 ng mL^{-1}) in PBS containing 3.0 mmol L^{-1} H_2O_2; (B), (D) The calibration curves between the currents and the concentrations of mucin 1. The measurements were repeated 3 times to obtain the standard deviation. (Amplitude: 50 mV, pulse width: 0.050 s, step potential: 5.0 mV).

Gr@PdPtNPs/GCE with different mucin 1 concentrations were recorded by DPV and chronoamperometry respectively. Fig. 3A illustrates the DPV of the dDNA/H-Gr@PdPtNPs/GCE incubated in different mucin 1 solutions. The peak currents of DPV increased with the increase of mucin 1 concentration which possibly due to mucin 1-MUC1a complex left from the electrode causing improved electron transfer. As shown in Fig. 3B, the calibration plot displays a good linear relationship between the peak currents and the logarithm concentrations of mucin 1 in the range from 8.0 pg mL^{-1} to 80 ng mL^{-1}. The linear regression equation is ΔI (μA) = 4.033 log c +11.8 (R^2 = 0.9978) and the limit of detection (S/N = 3) is 2.5 pg mL^{-1}. The performance of dDNA/H-Gr@PdPtNPs/GCE towards the determination of mucin 1 was also evaluated by chronoamperometry. Fig. 3C depicts the chronoamperometry of the biosensor for different mucin 1 concentrations in 0.10 mol L^{-1} PBS containing 3.0 mmol L^{-1} H_2O_2. The currents increased with the increase of mucin 1 concentration which attributed to the improved electrocatalytic activity of H-Gr@PdPtNPs for H_2O_2 reduction when mucin 1-MUC1a complex left from the electrode. The linear ranges of the reduction currents of H_2O_2 is from 0.8 pg mL^{-1} to 80 ng mL^{-1} and the linear regression equation is ΔI (μA) = 23.6 log c +97 (R^2 = 0.9983) (Fig. 3D). The limit of detection for mucin 1 (S/N = 3) is 0.25 pg mL^{-1} which was comparable with the previous reported mucin 1 sensor. The

Table 1
The comparison of different analytical methods for mucin 1 detection.

Platform	Assay	LOD	Linearity range	Reference
L-DNA/Exo I-assisted aptasensor	DPV	0.40 pg mL^{-1}	1.0 pg mL^{-1}-50 ng mL^{-1}	Lin et al. (2018)
Photoluminescence- quenching nanopaper	fluorescence	0.0113 pg mL^{-1}	0.0113–113 pg mL^{-1}	Liu et al. (2019)
521-MOF nanosheets aptasensor	EIS, SPR	0.12, 0.65 pg mL^{-1}	0.001–0.5 ng mL^{-1}	He et al. (2017)
ISP/AuNPs-based aptasensor	SWV	2.0566 fg mL^{-1}	0.0057–1.13 pg mL^{-1}	Xiang et al. (2017)
Ag/AuNCs/GO aptasensor	fluorescence	0.18 ng mL^{-1}	1.33–200 ng mL^{-1}	Wang et al. (2018)
AuNPs-PEI@Ru–PCN-777 immunosensor	ECL	33.3 fg mL^{-1}	0.1 pg mL^{-1}-100 ng mL^{-1}	Hu et al. (2018)
dDNA/H-Gr@PdPtNPs aptasensor	DPV chronoamperometry	2.5 pg mL^{-1} 0.25 pg mL^{-1}	8.0 pg mL^{-1}-80 ng mL^{-1} 0.8 pg mL^{-1}-80 ng mL^{-1}	This work

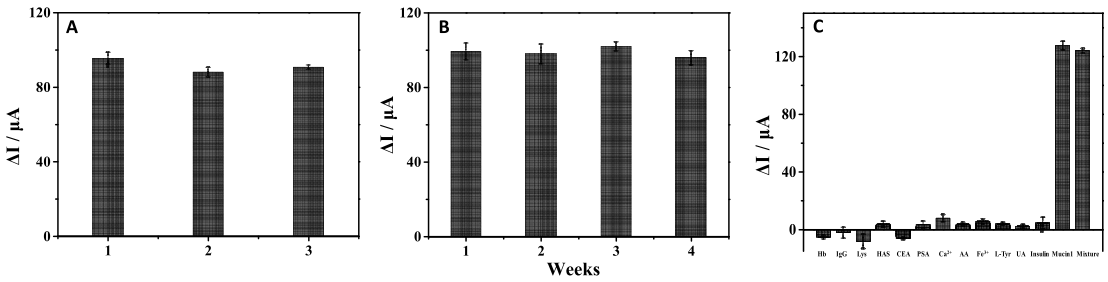

Fig. 4. (A) Reproducibility and (B) stability of the dDNA/H-Gr@PdPtNPs/GCE aptasensor in 8.0 ng mL^{-1} mucin 1 containing 3.0 mmol L^{-1} H_2O_2. (C) Selectivity of the aptasensor in 80 ng mL^{-1} mucin 1 containing 3.0 mmol L^{-1} H_2O_2. Error bars show the standard deviations of measurements taken from 3 times.

detailed specific characteristics are shown in Table 1. The wide linear ranges and low detection limits may be benefit from the outstanding conductivity and peroxidase-like activity of the modified materials, the abundance of binding affinities and the synergistic catalysis effect of H-Gr and PdPtNPs. The aptasensor will be a promising candidate for biomarker detection.

3.6. Reproducibility, stability and selectivity of dDNA/H-Gr@PdPtNPs/GCE

The reproducibility of the aptasensor was quantified by repetitively fabricated with the same glassy carbon electrode for 3 times and the peak current were recorded in 8.0 ng mL^{-1} mucin 1 solution (in Fig. 4A). The relative standard deviation (RSD) was calculated to be 5.0%, which indicated an acceptable reproducibility for mucin 1 detection.

To evaluate the stability, the as-prepared dDNA/H-Gr@PdPtNPs/GCE was stored at 4 °C for four weeks and the DPV signal was recorded in 0.10 mol L^{-1} PBS. The peak current maintained 97.1% of the original response, which suggests the aptasensor had satisfied stability (in Fig. 4B).

The selectivity of the proposed assay strategy was investigated by detecting some the interference such as Hb, IgG, Lys, HSA, CEA, PSA, Ca^{2+}, Fe^{3+}, UA, AA, L-Tyr, insulin peptide and the mixture under the same condition. As shown in Fig. 4C, the developed aptasensor exhibited a remarkable peak current change to 80 ng mL^{-1} mucin 1, while the peak current changes were negligible after addition of the above interference though their concentrations were 50 times (4.0 μg mL^{-1}) of mucin 1. In addition, the cross reactivity (CR) of mucin 1 and its analogues (mucin 4, mucin 16, mucin 20) were also studied to evaluate the selectivity of the electrochemical aptasensor. The concentrations of analytes corresponding to 50% current change to the aptasensor (EC_{50}) was used to estimate the CR. Firstly, the current responses of the sensor to varying concentrations of targets were normalized to fit the range 0–100%. Then, the percent current changes to varying concentrations of targets were plotted with the concentration of targets, and EC_{50} was calculated by non-linear fitting function. The respective EC_{50} values for mucin 1, mucin 4, mucin 16 and mucin 20 were 0.15 ng mL^{-1}, 8450 ng mL^{-1}, 5466 ng mL^{-1}, 5143 ng mL^{-1}. The CR of mucin 1, mucin 4, mucin 16, mucin 20 with aptamer were calculated to be 100%, 0.0018%, 0.0029%, 0.0030% respectively, which indicates no significant CR between mucin 1 and its analogues (As is shown in Fig. S5). The results demonstrate that this method had good specificity.

3.7. The practicability of the aptasensor

The reliability and feasibility of the proposed aptasensor were estimated in health human blood serum under the optional experimental conditions. In this procedure, the blood samples were diluted 100-fold by PBS to reduce the matrix effect. Then different concentrations of mucin 1 were added into the prepared human serum samples and determined by the standard addition method. The results are listed in Table S1, the recoveries are ranging from 95% to 104.2% which demonstrate that the aptasensor had good accuracy for the detection of mucin 1 in practical samples.

4. Conclusion

In conclusion, a novel dual signal and label-free electrochemical aptasensor based on H-Gr@PdPtNPs was fabricated for mucin 1 determination with wide linear range, low detection limit as well as high stability and selectivity. The superior sensing performance mainly benefits from following four points: 1) Hemin attached on the graphene surface avoided graphene aggregation and acted as an in-situ electrochemical signal probe for DPV detection. Moreover, the high peroxidase activity of hemin can catalyze H_2O_2 reduction and recorded with chronoamperometry. 2) The introduction of PdPtNPs can enhance the electron transfer and provide more accessible binding sites for anchoring the dDNA. 3) The synergistic effects of H-Gr, PdPtNPs effectively increase the electrocatalytic properties, the conductivity and specific surface area. 4) The high affinity between mucin 1 and its aptamer realized the specific recognition. Hence, it can be expected as an alternative analytical method to distinguish mucin 1 in real clinical diagnostics.

Credit author statement

Guojuan Zhang, The author is responsible for the nanomaterial synthesis and characterization, electrochemical measurements and original draft writing, Zhiguang Liu, The author is credited for the data analysis and presentation, Lifang Fan, The author is responsible for

designing the aptasensor construction and helping in interpretation of obtained data, Yujie Han, The author is credited for verification the experiment, Yujing Guo, The author is responsible for conceptualization and supervision of the project, and reviewing and editing the draft.

Declaration of competing interest

The authors declare that they have no known competing financial interests or personal relationships that could have appeared to influence the work reported in this paper.

Acknowledgements

This research work was supported by the National Natural Science Foundation of China (No. 21775095, 21707082), the Young "Sanjin" Scholar Foundation of Shanxi Province (No. 2016768) and the Scientific and Technological Key Project of Shanxi Province (No.20191102005).

Appendix A. Supplementary data

Supplementary data related to this article can be found at https://doi.org/10.1016/j.bios.2020.112785.

References

Apostolopoulos, V., Pietersz, G.A., Tsibanis, A., Tsikkinis, A., Drakaki, H., Loveland, B.E., Piddlesden, S.J., Plebanski, M., Pouniotis, D.S., Alexis, M.N., McKenzie, I.F., Vassilaros, S., 2006. Breast Cancer Res. 8 (3).
Cao, Y., Dai, Y., Chen, H., Tang, Y., Chen, X., Wang, Y., Zhao, J., Zhu, X., 2019. Biosens. Bioelectron. 130, 132–138.
Chen, G., Jin, M., Ma, J., Yan, M., Cui, X., Wang, Y., Zhang, X., Li, H., Zheng, W., Zhang, Y., Abd El-Aty, A.M., Hacımüftüoğlu, A., Wang, J., 2020. J. Agric. Food Chem. 68 (2), 660–668.
Chen, T., Xu, J., Yang, P., Sheng, Q., Zheng, J., Cao, W., Yue, T., Zhou, M., Wang, C., 2019. Sensor. Actuator. B Chem. 298.
Chen, X., Zhang, Q., Qian, C., Hao, N., Xu, L., Yao, C., 2015. Biosens. Bioelectron. 64, 485–492.
Cheng, A.K.H., Su, H., Wang, A., Yu, H., 2009. Anal. Chem. 81 (15), 6130–6139.
Falahat, R., Wiranowska, M., Gallant, N.D., Toomey, R., Hill, R., Alcantar, N., 2015. Cell. Immunol. 298 (1–2), 96–103.
Fan, C., Liu, J., Zhao, H., Li, L., Liu, M., Gao, J., Ma, L., 2019. RSC Adv. 9 (58), 33678–33683.
Ge, S., Zhao, J., Wang, S., Lan, F., Yan, M., Yu, J., 2018. Biosens. Bioelectron. 102, 411–417.
Gheybi, E., Amani, J., Salmanian, A.H., Mashayekhi, F., Khodi, S., 2014. Tumor Biol. 35 (11), 11489–11497.
Guo, Y., Deng, L., Li, J., Guo, S., Wang, E., Dong, S., 2011a. ACS Nano 5 (2), 1282–1290.
Guo, Y., Li, J., Dong, S., 2011b. Sensor. Actuator. B Chem. 160 (1), 295–300.
Hatami, Z., Jalali, F., Tabrizi, M.A., Shamsipur, M., 2019. Biosens. Bioelectron. 141.
He, L., Duan, F., Song, Y., Guo, C., Zhao, H., Tian, J., Zhang, Z., Liu, C., Zhang, X., Wang, P., Du, M., Fang, S., 2017. 2D Mater. 4 (2).
Hu, G., Xiong, C., Liang, W., Zeng, X., Xu, H., Yang, Y., Yao, L., Yuan, R., Xiao, D., 2018. ACS Appl. Mater. Interfaces 10 (18), 15913–15919.
Hummers, W.S., Offeman, R.E., 1958. J. Am. Chem. Soc. 80 (6), 1339-1339.
Jiang, X., Wang, H., Wang, H., Zhuo, Y., Yuan, R., Chai, Y., 2017. Anal. Chem. 89 (7), 4280–4286.
Kimmel, D.W., LeBlanc, G., Meschievitz, M.E., Cliffel, D.E., 2012. Anal. Chem. 84 (2), 685–707.
Kufe, D.W., 2009. Nat. Rev. Canc. 9 (12), 874–885.
Li, S., Liu, Z., Li, J., Chen, A., Chai, Y., Yuan, R., Zhuo, Y., 2018. ACS Appl. Mater. Interfaces 10 (17), 14483–14490.
Lin, C., Zheng, H., Huang, Y., Chen, Z., Luo, F., Wang, J., Guo, L., Qiu, B., Lin, Z., Yang, H., 2018. Biosens. Bioelectron. 117, 474–479.
Liu, J., Cui, M., Niu, L., Zhou, H., Zhang, S., 2016. Chem. Eur J. 22 (50), 18001–18008.
Liu, S., Xu, N., Tan, C., Fang, W., Tan, Y., Jiang, Y., 2018a. Anal. Chim. Acta 1018, 86–93.
Liu, W., Hiekel, K., Huebner, R., Sun, H., Ferancova, A., Sillanpaa, M., 2018b. Sensor. Actuator. B Chem. 255, 1325–1334.
Liu, Y., Mao, G., Wang, W., Tian, S., Ji, X., Liu, M., He, Z., 2019. Chem. Commun. 55 (18), 2660–2663.
Ma, C., Liu, H., Zhang, L., Li, H., Yan, M., Song, X., Yu, J., 2018. Biosens. Bioelectron. 99, 8–13.
Mourya, S., Kumar, A., Jaiswal, J., Malik, G., Kumar, B., Chandra, R., 2019. Sensor. Actuator. B Chem. 283, 373–383.
Nie, C., Ma, L., Li, S., Fan, X., Yang, Y., Cheng, C., Zhao, W., Zhao, C., 2019. Nano Today 26, 57–97.
Song, H., Zhang, X., Liu, Y., Su, Z., 2019. Chem. Rec. 19 (2–3), 534–549.
Themsirimongkon, S., Ounnunkad, K., Saipanya, S., 2018. J. Colloid Interface Sci. 530, 98–112.
Wang, H., Sun, J., Lu, L., Yang, X., Xia, J., Zhang, F., Wang, Z., 2020. Anal. Chim. Acta 1094, 18–25.
Wang, J., Zhang, S., Dai, H., Zheng, H., Hong, Z., Lin, Y., 2019a. Biosens. Bioelectron. 142.
Wang, W., Tang, H., Wu, Y., Zhang, Y., Li, Z., 2019b. Biosens. Bioelectron. 132, 217–223.
Wang, M., Hu, B., Ji, H., Song, Y., Liu, J., Peng, D., He, L., Zhang, Z., 2017. ACS Omega 2 (10), 6809–6818.
Wang, Q., Zhou, Z., Zhai, Y., Zhang, L., Hong, W., Zhang, Z., Dong, S., 2015. Talanta 141, 247–252.
Wang, Y., Wang, S., Lu, C., Yang, X., 2018. Sensor. Actuator. B Chem. 262, 9–16.
Xiang, J., Pi, X., Chen, X., Xiang, L., Yang, M., Ren, H., Shen, X., Qi, N., Deng, C., 2017. Biosens. Bioelectron. 96, 268–274.
Xu, G., Hou, J., Zhao, Y., Bao, J., Yang, M., Fa, H., Yang, Y., Li, L., Huo, D., Hou, C., 2019. Sensor. Actuator. B Chem. 287, 428–436.
Yang, S., Zhang, F., Liang, Q., Wang, Z., 2018. Biosens. Bioelectron. 120, 85–92.
Zhang, G., Liu, Z., Fan, L., Guo, Y., 2018. Microchim. Acta 185 (3).
Zhang, T., Xing, Y., Song, Y., Gu, Y., Yan, X., Lu, N., Liu, H., Xu, Z., Xu, H., Zhang, Z., Yang, M., 2019a. Anal. Chem. 91 (16), 10589–10595.
Zheng, J., Peng, X., Wang, Y., Bao, T., Wen, W., Zhang, X., Wang, S., 2019b. Anal. Chim. Acta 1086, 75–81.
Zhang, Z., Hui, J., Guo, Z., Yu, Q., Xu, B., Zhang, X., Liu, Z., Xu, C., Gao, J., Wang, X., 2012. Nanoscale 4 (8), 2633–2639.